ELSEVIER

Journal of Fluids and Structures 25 (2009) 304–320

JOURNAL OF FLUIDS AND STRUCTURES

www.elsevier.com/locate/jfs

Effect of uncertainty on the bifurcation behavior of pitching airfoil stall flutter

S. Sarkar[a,*], J.A.S. Witteveen[b], A. Loeven[b], H. Bijl[b]

[a]*Department of Aerospace Engineering, IIT Madras, Chennai 600036, India*
[b]*Faculty of Aerospace Engineering, Delft University of Technology, Kluyverweg 1, 2629 HS Delft, The Netherlands*

Received 17 April 2007; accepted 11 June 2008

Abstract

In this paper the effect of system parametric uncertainty on the stall flutter bifurcation behavior of a pitching airfoil is studied. The aerodynamic moment on the two-dimensional rigid airfoil with nonlinear torsional stiffness is computed using the ONERA dynamic stall model. The pitch natural frequency, a cubic structural nonlinearity parameter, and the structural equilibrium angle are assumed to be uncertain. The effect on the amplitude of the response, the bifurcation of the probability distribution, and the flutter boundary is considered. It is demonstrated that the system parametric uncertainty results already in 5% probability of pitching stall flutter at a 12.5% earlier position than the point where a deterministic analysis would predict unstable behavior. Probabilistic collocation is found to be more efficient than the Galerkin polynomial chaos method and Monte Carlo simulation for modeling uncertainty in the post-bifurcation domain.

Keywords: Stall flutter; Uncertainty quantification; Galerkin polynomial chaos; Probabilistic collocation; Flutter boundary

1. Introduction

It is increasingly acknowledged that flutter analysis should include the quantification of the effects of system parametric uncertainty. Dynamical systems are known to be sensitive to physical uncertainties, since they often amplify this random variability with time. A stable response of a nonlinear dynamical system can change at a bifurcation boundary into an oscillatory instability that can grow in an unbounded fashion, which is known as flutter (Fung, 1955). Flutter of aircraft and rotor structures is of practical interest to engineers, since it can lead to fatigue damage or failure of the structure. System parametric uncertainties can significantly affect the onset and properties of flutter. The added value of modeling these uncertainties with probabilistic methods compared to deterministic approaches to robustness is that they quantify the effect of uncertainties in a probabilistic sense. Based on the resulting detailed probabilistic information well-balanced decisions can be made in a robust design optimization process.

Monte Carlo (MC) simulation and perturbation techniques are classical probabilistic methods for uncertainty quantification. However, stochastic spectral methods based on the polynomial chaos expansion may be more efficient and accurate alternatives. The polynomial chaos expansion by Wiener (1938) is a polynomial expansion in probability

*Corresponding author. Tel.: +91 442 257 4024; fax: +91 442 257 4002.
E-mail address: sunetra.sarkar@gmail.com (S. Sarkar).

0889-9746/$ - see front matter © 2008 Elsevier Ltd. All rights reserved.
doi:10.1016/j.jfluidstructs.2008.06.006

space in terms of independent random variables and deterministic coefficients. The Galerkin polynomial chaos (GPC) method proposed by Ghanem and Spanos (1991) employs a Galerkin stochastic finite element approach to solve for the deterministic coefficients. The Galerkin projection in probability space results in a coupled set of deterministic equations. This type of methods are called intrusive methods, since the deterministic solver has to be altered to solve for the coupled equations. The method can achieve exponential convergence for Gaussian distributions, since it is based on Gaussian random variables and Hermite polynomials (Ghanem, 1999). The exponential convergence has been extended to more distributions in the generalized polynomial chaos by Xiu and Karniadakis (2002) and for arbitrary distributions by Wan and Karniadakis (2006a) and Witteveen and Bijl (2006a). Other nonpolynomial expansions are the wavelet based Wiener–Haar expansion of Le Maître et al. (2004) and the Fourier-chaos expansion of Millman et al. (2003).

In order to avoid solving the coupled set of equations of the GPC method intrusively, several nonintrusive uncoupled alternatives have been proposed. In nonintrusive polynomial chaos methods a deterministic solver is used as a black-box like in MC simulation. The probabilistic collocation (PC) method is such a nonintrusive polynomial chaos method in which the deterministic coefficients are solved for by collocating the problem in Gauss points in probability space (Babuska et al., 2007; Loeven et al., 2007). Suitable Gauss points are the zeros of polynomials orthogonal with respect to the probability density of the uncertain system parameter. Exponential convergence with respect to the order of approximation can be obtained for arbitrary probability distributions. Babuska et al. (2007) have proven that for elliptic partial differential equations the PC method is equivalent to the GPC method. The nonintrusive polynomial chaos method proposed by Hosder et al. (2006) and Walters (2003) is based on approximating the polynomial chaos coefficients. A similar approach called nonintrusive spectral projection is used by Reagan et al. (2003). The stochastic collocation method proposed by Mathelin and Hussaini (2003) and Mathelin et al. (2005) showed a significant decrease in computational time compared to the GPC method. When multiple uncertain parameters are involved the collocation grids are constructed using tensor products of one-dimensional quadrature grids. The amount of collocation point, and therefore the number of required deterministic solves, increases rapidly. As an alternative, sparse grid collocation approaches are used (Ganappathysubramanian and Zabaras, 2007; Gerstner and Griebel, 1998; Xiu and Hesthaven, 2005).

Although polynomial chaos methods have been successful in many problems, often MC simulation or perturbation techniques are used for modeling uncertainty in flutter analysis. MC simulations have, for example, been used by Lindsley et al. (2002, 2006) to study the periodic response of nonlinear plate equations under supersonic flow subject to uncertain modulus of elasticity and boundary conditions. The effect of uncertainties on panel flutter has been analyzed by Liaw and Yang (1993) using a second moment perturbation based stochastic finite element model. A first order perturbation method has been applied to a bending-torsion flutter model in an unpublished report by Poirion [see Lind and Brenner (1998) and Pettit (2004a)], to predict flutter probability with uncertain structural mass and stiffness. Poirion (2000) has also investigated nonlinear random oscillations with application to aeroservoelastic systems using simulation techniques for Gaussian and non-Gaussian random processes and random delay modeling of control systems. Poirel and Price (2003) have solved random bending-torsion flutter equations under turbulent flow conditions with a linear structural model using a MC type approach. Choi and Namachchivaya (2006) have found qualitatively different response density functions in nonlinear panel flutter under supersonic flow subject to random fluctuations in the turbulent boundary layer using nonstandard reduction through stochastic averaging. Ibrahim et al. (2005) and Beloiu et al. (2005) have investigated the effects of boundary condition and joint condition uncertainties on a panel flutter system. De Rosa and Franco (2008) have presented the response of a plate subjected to stochastic flow-field due to the effect of turbulent boundary layer using numerical and analytical approach. Pettit (2004a, b) has outlined that small uncertainties in the system parameters, external loads and boundary conditions can significantly modify the static and dynamic aeroelastic system response. Various uncertain aeroelastic analyses for plate-like structures are discussed in Dowell et al. (1989) and Nigam and Narayanan (1994).

Studies that use polynomial chaos methods to predict the effect of uncertainties in flutter analysis report that the polynomial chaos expansion can have difficulty capturing the uncertain response after long-term time integration. Pettit and Beran (2004, 2006) have found that the Wiener–Hermite expansion suffers from energy loss in representing the periodic response of bending-torsion flutter model for long integration times. For the wavelet based Wiener–Haar expansion of Le Maître et al. (2004), this problem is less dominant (Pettit and Beran, 2006). Millman et al. (2003) demonstrated that a Fourier-chaos expansion can be computationally more efficient for a bending-torsion flutter problem subjected to Gaussian distributions than the regular Wiener–Hermite expansion. Lucor and Karniadakis (2004) and Wan and Karniadakis (2006b) have observed that the effect of uncertainties on the frequency of the response is of major influence on long-term integration accuracy of polynomial chaos approximations.

In this paper, the effect of parametric uncertainty on the stall flutter behavior of a pitching airfoil is studied using polynomial chaos expansion methods. This study can be considered a qualitative assessment of the effect of uncertainty

on the bifurcation behavior of the system. Stall flutter is, for example, of interest to wind turbine research community. In the present deterministic model, the blade structure is modeled as a two-dimensional rigid airfoil with torsional degree-of-freedom. The structural stiffness (Fragiskatos, 1999) in the torsional direction is modeled using a combination of a linear and a cubic nonlinear spring (Lee and Tron, 1989; Lee et al., 1999), since a blade section which is being twisted is likely to behave as a cubic stiffness hardening spring (Lee et al., 1999). The stall aerodynamic moment is computed using the ONERA semi-empirical dynamic stall model as shown by Beedy et al. (2003) and Dunn and Dugundji (1992). This approach is commonly used in many engineering aeroelastic applications (Lee et al., 1999; Sheta et al., 2002; Tang and Dowell, 1993a, b). Tang and Dowell (2004) have also used the ONERA dynamic stall model to investigate the effects of structural nonlinearity on a high aspect ratio binary wing flutter. In another recent work, Svácek et al. (2007) have investigated two-dimensional flutter in the dynamic stall regime; however, they have not used a semi-empirical model to compute the aerodynamic loads, but with a finite element based discretization of the Navier–Stokes equations.

An earlier deterministic study by Sarkar and Bijl (2008) on a stall flutter system has pointed out that the response is sensitive to model parameter variations. In this paper the GPC method and the PC method are applied to study the effect of uncertainty in several model parameters. The pitch natural frequency, the cubic structural nonlinearity parameter, and the structural equilibrium angle are assumed to be uncertain.

The efficiency of both the GPC method and the PC method are compared for the case with the uncertain pitch natural frequency. The effect of the polynomial chaos expansion order on the accuracy of the long-term time integration results is studied. A comparison of the computational costs of the two methods shows that the PC method is more efficient for the highly nonlinear model. The PC method is further employed to study the effect of the uncertain cubic structural nonlinearity parameter and the structural equilibrium angle on the bifurcation behavior of the system. In these cases the effect on the amplitude of the response, the bifurcation of the probability distribution, and the flutter boundary is considered.

The polynomial chaos method and the PC method are briefly reviewed in Section 2. In Section 3 the equation of motion and the aerodynamic model for the stall flutter problem are given. Numerical results are presented in Section 4 and the conclusions are summarized in Section 5.

2. Polynomial chaos expansion methods

Modeling uncertainties in the stall flutter problem results in a system of stochastic differential equations based on a probability space $(\Omega, \mathscr{F}, P)$. Let $\omega \in U(0,1)$ be an element of the sample space Ω, $\mathscr{F} \subset 2^{\Omega}$ the σ-algebra of events and P a probability measure. Random event ω is defined as uniformly distributed on $[0,1]$ in accordance with the standard technique for generating random numbers of an arbitrary distribution by projecting uniformly distributed numbers ω onto probability measure P, as in Bhattacharya and Waymire (2007). The argument ω is used for an uncertain variable $u(t,\omega)$ to emphasize the fact that an uncertain variable is a function of a random event. Suppose that the stall flutter model is described by the following equation for $u(t,\omega)$ with an nonlinear operator $\mathscr{L}$ and a source term S,

$$\mathscr{L}(t,\omega;u(t,\omega)) = S(t,\omega). \tag{1}$$

Let us consider the operator to be a differential operator and the system is described by a nonlinear stochastic differential equation for $u(t,\omega)$ with a nonlinear function $g(u(t,\omega))$

$$\frac{\mathrm{d}(u(t,\omega))}{\mathrm{d}t} + c_1(\omega)u(t,\omega) + c_2(\omega)g(u(t,\omega)) = f(t), \tag{2}$$

with time t and appropriate initial conditions. The system is assumed to have parametric uncertainty through c_1, c_2 with known probability distribution. The GPC method and the PC method to propagate the uncertainty through (1) are discussed in this section.

2.1. GPC method

The uncertain variable $u(t,\omega)$ and the uncertain parameter can be represented by a polynomial chaos expansion

$$u(t,\omega) = \sum_{i=0}^{\infty} u_i(t)\Psi_i(\xi(\omega)), \tag{3}$$

where $\{u_i(t)\}$ denotes the deterministic polynomial chaos coefficients and $\{\Psi_i(\xi(\omega))\}$ denotes orthogonal polynomials in terms of a random variable $\xi(\omega)$. The random variable $\xi(\omega)$ is obtained from a linear transformation of the uncertain

physical parameter to a corresponding standard domain, i.e. $[-1,1]$, $[0,\infty)$ or $(-\infty,\infty)$. The polynomials $\{\Psi_i(\xi(\omega))\}$ satisfy the following orthogonality relation:

$$\langle \Psi_i(\xi), \Psi_j(\xi)\rangle = \int_{\mathrm{supp}_\xi} \Psi_i(\xi)\Psi_j(\xi) w_\xi(\xi)\,\mathrm{d}\xi = \langle \Psi_i^2(\xi)\rangle \delta_{ij}, \tag{4}$$

where δ_{ij} denotes the Kronecker delta and $\langle\cdot,\cdot\rangle$ denotes an inner product, $w_\xi(\xi)$ is a weighting function, and supp_ξ is the support of $\xi(\omega)$. To be able to obtain exponential convergence for sufficiently smooth solutions, the weighting function of the integration is chosen to be equal to the probability density $f_\xi(\xi)$ of $\xi(\omega)$, i.e. $w_\xi(\xi) = f_\xi(\xi)$ (Wan and Karniadakis, 2006a; Witteveen and Bijl, 2006a).

The deterministic coefficients $\{u_i(t)\}$ in (3) can be solved for numerically using a stochastic finite element approach, as shown by Ghanem and Spanos (1991). For the numerical implementation the infinite summation in ξ in (3) is replaced by a truncated finite-term summation

$$u(t,\omega) = \sum_{i=0}^{N} u_i(t)\Psi_i(\xi(\omega)). \tag{5}$$

We also assume,

$$c_{1,2} = \sum_{i=0}^{1} c_{1,2i}\Psi_i(\xi(\omega)). \tag{6}$$

Substituting the above into the governing Eq. (2), we obtain

$$\sum_{i=0}^{N} \frac{\mathrm{d}}{\mathrm{d}t} u_i\Psi_i + \sum_{j=0}^{1}\sum_{i=0}^{N} u_i c_{1j}\Psi_i\Psi_j + \sum_{j=0}^{1} c_{2j} g\left(\sum_{i=0}^{N} u_i\Psi_i\right) = f(t). \tag{7}$$

For $g(u)$ being a cubic nonlinear function, $g(\sum_{i=0}^{N} u_i\Psi_i)$ will take the following form:

$$g(u) = u^3 = \left(\sum_{i=0}^{N} u_i\Psi_i\right)^3 = \sum_{i1=0}^{N}\sum_{i2=0}^{N}\sum_{i3=0}^{N} u_{i1}\Psi_{i1}u_{i2}\Psi_{i2}u_{i3}\Psi_{i3}. \tag{8}$$

A stochastic Galerkin projection is employed to obtain a system of coupled $N+1$ deterministic equations for the $N+1$ deterministic coefficients. The Galerkin projection in probability space of (7) onto each polynomial basis $\{\Psi_k(\xi(\omega))\}_{k=0}^{N}$ in the sense of inner product (4) yields

$$\left\langle \left[\sum_{i=0}^{N} \frac{\mathrm{d}}{\mathrm{d}t} u_i\Psi_i + \sum_{i=0}^{N}\sum_{j=0}^{1} u_i c_{1j}\Psi_i\Psi_j + \sum_{j=0}^{1} c_{2j} g\left(\sum_{i=0}^{N} u_i\Psi_i\right)\right], \Psi_k(\xi)\right\rangle = \langle f(t), \Psi_k(\xi)\rangle, \tag{9}$$

for $k = 0, 1, \ldots, N$. The Galerkin projection results in a coupled set of $N+1$ deterministic equations:

$$\frac{\mathrm{d}u_k}{\mathrm{d}t} + \frac{1}{\langle\Psi_k^2\rangle}\sum_{j=0}^{1}\sum_{i=0}^{N} u_i c_{1j}\langle\Psi_i\Psi_j\Psi_k\rangle + \left\langle \left[\sum_{j=0}^{1} c_{2j} g\left(\sum_{i=0}^{N} u_i\Psi_i\right)\right], \Psi_k(\xi)\right\rangle = \langle f(t), \Psi_k(\xi)\rangle. \tag{10}$$

The inner product term $\langle\Psi_i\Psi_j\Psi_k\rangle$ along with $1/\langle\Psi_k^2\rangle$ can be evaluated analytically. For analytic nonlinearities like a cubic function shown in (8), the third term in the left-hand side of (10) will also have inner product terms which can be evaluated analytically before the time marching process. For nonanalytic forms the term needs to be evaluated numerically using some numerical integration process like Simpson's rule, etc.

The original homogeneous polynomial chaos (Ghanem and Spanos, 1991) is based on a Gaussian probability measure P and a Gaussian random variable $\xi(\omega)$. For that case Hermite polynomials satisfy orthogonality relation (4). For any arbitrary distributions the orthogonal polynomials are constructed using other classical polynomials or an orthogonalization method (Wan and Karniadakis, 2006a; Witteveen and Bijl, 2006a; Xiu and Karniadakis, 2002). In this work the uncertain system parameters are assumed to be lognormally distributed. A lognormal distribution is often a good model for nonnegative physical parameters. The orthogonal polynomials $\{\Psi_i(\xi(\omega))\}_{i=0}^{N}$ are constructed using Gram–Schmidt orthogonalization (Gautschi, 2004), in which the inner products are written as summations of the analytically known raw moments of the lognormal distribution. Constructing the polynomials in this way results in negligible additional computational costs compared to using classical polynomials.

2.2. PC method

Another approach to obtain a polynomial chaos approximation of the uncertain response $u(t,\omega)$ is the PC method of Babuska et al. (2007) [also see Loeven et al. (2007)]. In this nonintrusive approach the polynomial chaos coefficients are computed by solving uncoupled deterministic problems for various parameter values. The uncertain system parameter is written in terms of an Nth order polynomial chaos expansion with Lagrange basis polynomials $\{h_i(\xi(\omega))\}$

$$u(t,\omega)=\sum_{i=1}^{N+1}u_i^*(t)h_i(\xi(\omega)), \tag{11}$$

where $\{u_i^*(t)\}_{i=1}^{N+1}$ are the realizations of $u(t,\omega)$ at the $N+1$ collocation points $\{\xi_i\}_{i=1}^{N+1}$, with $\xi_i=\xi(\omega_i)$. The Lagrange interpolating polynomial chooses $\{h_i(\xi(\omega))\}_{i=1}^{N+1}$ of order N through the collocation points $\{\xi_i\}$ are given by

$$h_i(\xi(\omega))=\prod_{\substack{j=1\\ j\neq i}}^{N+1}\frac{\xi(\omega)-\xi_j}{\xi_i-\xi_j}, \tag{12}$$

such that $h_i(\xi_j)=\delta_{ij}$. Suitable collocation points are the Gaussian quadrature points corresponding to the inner product (4) with weighting function $w_\xi(\xi)=f_\xi(\xi)$. These collocation points are the roots of the orthogonal polynomial $\Psi_{N+2}(\xi(\omega))$ given by (4). The Gauss quadrature points can be computed for any arbitrary distributions using, for example, the Golub–Welsch algorithm, as shown by Golub and Welsch (1969). This algorithm employs the recurrence coefficients (Gautschi, 2005) of the orthogonal polynomials $\{\Psi_i(\xi)\}$.

The uncoupled set of $N+1$ equations for the deterministic coefficients $\{u_i^*(t)\}_{i=1}^{N+1}$ can be derived by substituting expansion (11) into the governing Eq. (2):

$$\frac{\mathrm{d}}{\mathrm{d}t}\left(\sum_{i=1}^{N+1}u_i^*(t)h_i(\xi)\right)+c_1(\omega)\sum_{i=1}^{N+1}u_i^*(t)h_i(\xi)+c_2(\omega)g\left(\sum_{i=1}^{N+1}u_i^*(t)h_i(\xi)\right)\approx f(t). \tag{13}$$

A Galerkin projection of each Lagrangian basis $\{h_j(\xi(\omega))\}_{j=1}^{N+1}$ results in

$$\left\langle\left(\frac{\mathrm{d}}{\mathrm{d}t}\left(\sum_{i=1}^{N+1}u_i^*(t)h_i(\xi)\right)+c_1(\omega)\sum_{i=1}^{N+1}u_i^*(t)h_i(\xi)+c_2(\omega)g\left(\sum_{i=1}^{N+1}u_i^*(t)h_i(\xi)\right)\right),h_j(\xi)\right\rangle=\langle f(t),h_j(\xi)\rangle, \tag{14}$$

for $j=1,2,\ldots,N+1$. Approximating the inner product in (14) using numerical integration and using property $h_i(\xi_j)=\delta_{ij}$ of the Lagrange polynomials results in the following set of uncoupled deterministic equations

$$\frac{\mathrm{d}(u_j^*(t))}{\mathrm{d}t}+c_1(\omega_j)u_j^*(t)+c_2(\omega_j)g(u_j^*(t))=f(t), \tag{15}$$

for $j=1,2,\ldots,N+1$. The distribution function can be constructed from the expansion coefficients $u_i^*(t)$ using expansion (11).

3. Stall flutter model

In this section the single-degree-of-freedom pitching airfoil stall flutter model is described. It consists of an equation of motion for the two-dimensional rigid airfoil with nonlinear torsional spring stiffness. The aerodynamic moment including the stall behavior is modeled using the ONERA dynamic stall model.

3.1. Equation of motion

A schematic plot of the two-dimensional blade section of unit span and the coordinate system is given in Fig. 1. The equation of motion for the single-degree-of-freedom pitching oscillation is given by Fragiskatos (1999) and Fung (1955):

$$I_\alpha\ddot{\alpha}+I_\alpha\omega_\alpha^2\alpha+K_{\mathrm{nl1}}\alpha^3=M(t). \tag{16}$$

Here, I_α is the wing mass moment of inertia, α is the effective angle of attack, ω_α is the natural frequency of the pitch elastic mode, K_{nl1} is a nonlinear stiffness term accounting for concentrated structural nonlinearities in the torsional direction, and $M(t)$ is the time dependent aerodynamic moment. A nondimensional form of the governing equation is

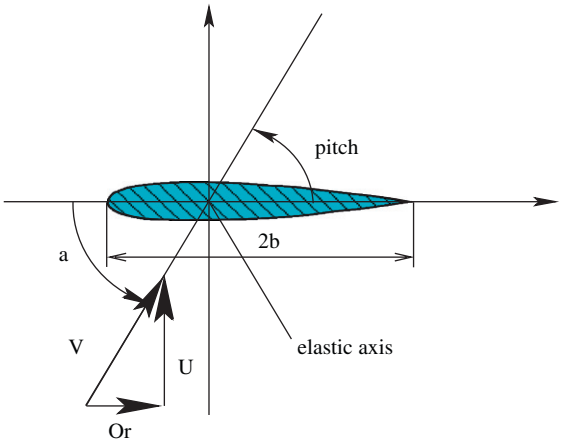

Fig. 1. Schematic plot of the airfoil coordinate system and oscillation degree-of-freedom.

often useful in aeroelastic analysis to investigate the effect of system parameters. The nondimensional form of (16) (Fragiskatos, 1999)

$$\alpha'' + \alpha/(U^2) + K_{\mathrm{nl}}\alpha^3 = 2C_m/(\pi\mu r_\alpha^2). \tag{17}$$

Here, $()'$ denotes a derivative with respect to nondimensional time $\tau = t\bar{V}/b$, $\bar{V}$ is the resultant velocity of the wind velocity U and the rotational velocity Ωr as shown in Fig. 1, b is the semi-chord of the blade, C_m is the aerodynamic moment coefficient, U is the nondimensional airspeed defined as $U = \bar{V}/b\omega_\alpha$, μ and r_α are nondimensional structural parameters, mass ratio $\mu = m/(\pi\rho b^2)$, radius of gyration $r_\alpha = I_\alpha/(mb^2)$, K_{nl} is the nondimensional form of K_{nl1}. Typical data for a 1000 KW capacity wind turbine are used with a semi-chord of $b = 0.8$ m at 0.75 blade radius and a representative resultant wind speed of $\bar{V} = 50$ m/s (Cheney and Migliore, 2000; Stiesdal, 1999).

The uncertain parameters in the structural model are the pitch natural frequency ω_α, the cubic structural nonlinearity parameter K_{nl}, and the structural equilibrium angle α_m. The uncertainty in ω_α is introduced in the model through U. The deterministic value of the structural nonlinearity K_{nl} is assumed to be zero. The parameter α_m is introduced in the same way as shown by Fragiskatos (1999) and Price and Fragiskatos (2000). The airfoil is given its initial perturbation about this angle. An extra moment is used to maintain this angle for the structure.

3.2. Aerodynamic stall model

The aerodynamic moment coefficient C_m in (17) is computed using the ONERA semi-empirical dynamic stall model, as shown in Beedy et al. (2003) and Dunn and Dugundji (1992). This model gives a system of ordinary differential equations for the aerodynamic loads. Using this type of semi-empirical aerodynamic models is common practice in engineering aeroelastic problems. The physical process of dynamic stall involves leading and trailing edge vortex development and their subsequent separation and shedding into the wake. Vortex growth increases suction and helps increase the aerodynamic loads beyond their static stall values. Vortex separation from the body triggers a rapid decrease of the loads. The ONERA model takes into account this complex unsteady phenomena step by step. A detailed discussion on the ONERA dynamic stall model is given by Dunn and Dugundji (1992) and Tran and Petot (1981). The differential equations are of the following form:

$$C_z = s_z\alpha' + k_{vz}\theta'' + C_{z_1} + C_{z_2}, \tag{18}$$

$$C'_{z_1} + \lambda_z C_{z_1} = \lambda_z(a_{0z}\alpha + \sigma_z\theta') + \alpha_z(a_{0z}\alpha' + \sigma_z\theta''), \tag{19}$$

$$C''_{z_2} + 2d\omega C'_{z_2} + w^2(1+d^2)C_{z_2} = -w^2(1+d^2)(\Delta C_z|\alpha + e\Delta C'_z|\alpha), \tag{20}$$

where the coefficients $s_z, k_{vz}, \lambda_z, \alpha_z, a_{0z}, \sigma_z, d, w$ and e are empirically determined by parameter identification techniques using experimental data. The values for the coefficients for the NACA0012 airfoil have been obtained from Dunn and Dugundji (1992). The pitch angle θ and the total angle of attack $\alpha = \theta - \bar{h}'$, are equal in this case since only torsional oscillations are considered. Here, $\bar{h}$ is the nondimensional flapping displacement normalized with the airfoil chord.

The coefficients C_z are the aerodynamic coefficient C_l, C_d or C_m for $z = \{l, d, m\}$. In this case, only the moment coefficient C_m is of interest. The aerodynamic moment consists of two contributions: (i) the inviscid circulatory part C_{m_1} given by (19) and (ii) the viscous stall part C_{m_2} given by (20), which becomes important above the static stall angle. The stall behavior is modeled in Eq. (20) by the ΔC_m term. The ΔC_m part is a nonlinear function which is identically zero below the static stall angle of 12° at which it exhibits a discontinuous step to a finite value.

The nonlinear ΔC_m term has a major influence on the implementation of the GPC method for the stall flutter model. The Galerkin projection (9) applied to the dynamic stall flutter model (17)–(20) results in inner products (4) containing nonlinear functions for the nonlinear terms involving K_{nl} and ΔC_m. The inner product with K_{nl} can be tabulated in a preprocessing step, since it contains polynomial nonlinearities only. The inner product of the terms containing ΔC_m involves a nonpolynomial nonlinearity in terms of a step function, which cannot be tabulated in a similar way. It is known that the application of the GPC formulation is difficult for nonpolynomial nonlinearities [see some proposed methods in Debusschere et al. (2004) and Witteveen and Bijl (2006b)]. Here the inner products containing ΔC_m are evaluated numerically using Simpson's rule at each time level. A trial and error approach has been used to select the sufficiently high number of integration points of 2500. The numerical integration contributes significantly towards making the coupled GPC approach much slower compared to nonintrusive PC method.

A fourth order Runge–Kutta scheme is used with a time step size of $\Delta\tau = 0.01$. This step size satisfies the criteria of convergence of the time integration technique and is also commensurate with the frequency of oscillation. The simulations are run up to $\tau = 800$, by which the transient effects are well past and the response reaches time stationarity. The simulation uses an initial perturbation of $\alpha_0 = 10^\circ$ about a structural equilibrium mean angle of attack of $\alpha_m = 4^\circ$.

4. Results

Numerical results are presented for the effect of uncertainty in three model parameters on the stall flutter response. Uncertainty in the pitch natural frequency ω_α, the cubic structural nonlinearity parameter K_{nl}, and the structural equilibrium angle α_m is considered. For the first uncertain parameter, ω_α, the GPC method and the PC method are compared. For the other two uncertain parameters, K_{nl} and α_m, the PC method is used, which proved to be the more efficient method for the current problem. GPC and PC results are compared with a 2500 point MC simulations. It is well known that MC results go to the exact solution asymptotically as the sample size becomes infinitely large. However, a very large sample size makes the computation prohibitively slow. In this work, sample size of 2500 is chosen based on the feasibility of the computational cost involved.

4.1. Comparison of GPC and PC for uncertain pitch natural frequency ω_α

GPC and PC are compared for two test cases with an uncertain pitch natural frequency ω_α. The uncertainty in ω_α effects the model through the bifurcation parameter U. The pitch natural frequency ω_α is varied corresponding to pre-bifurcation and post-bifurcation values of U separately.

4.1.1. Uncertain pitch natural frequency ω_α in the pre-bifurcation domain

The deterministic bifurcation plot with respect to bifurcation parameter U is given in Fig. 2. The bifurcation plot is given in terms of the maximum and minimum values of an oscillating response, which are those where the time derivative of the response $\alpha(\tau)$ is zero. The deterministic model shows a supercritical Hopf bifurcation at approximately $U = 16$, where the angle of attack of the damped response reaches the stall angle of 12°. In the pre-bifurcation domain the angle of attack at which the damped response stabilizes increases with U. Beyond the bifurcation point the system exhibits a periodic response, which is known as a limit cycle oscillation (LCO), with increasing amplitude as U increases.

The uncertainty of the nonnegative pitch natural frequency ω_α is described by a lognormal distribution with mean $\mu_{\omega_\alpha} = 6.25\,\mathrm{rad/s}$, with a coefficient of variation (CV) of $CV_{\omega_\alpha} = 1.5\%$. This corresponds to $U = 10$ using the test data of $\bar{V} = 50\,\mathrm{m/s}$ and $b = 0.8\,\mathrm{m}$, as was mentioned in Section 3.1. In Fig. 3 the distribution of ω_α and the corresponding U values are shown. The variation of U is well below the critical $U = 15.5$ value, such that $\alpha(\tau)$ exhibits a nonoscillatory damped solution.

The propagation of uncertainty through the model is computed using the GPC method and the PC method with a fourth order expansion with $N = 4$. In Fig. 4 the approximations of the distribution function of the response $\alpha(\tau)$ at $\tau = 800$ are compared to MC simulation results based on 2500 realizations. For this pre-bifurcation case, the results of GPC and PC both compare well with the MC results already for relatively low order expansions.

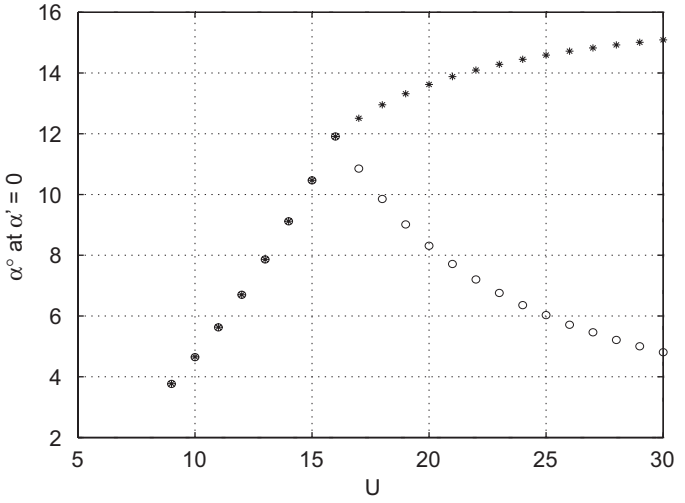

Fig. 2. Bifurcation diagram for the deterministic aeroelastic system.

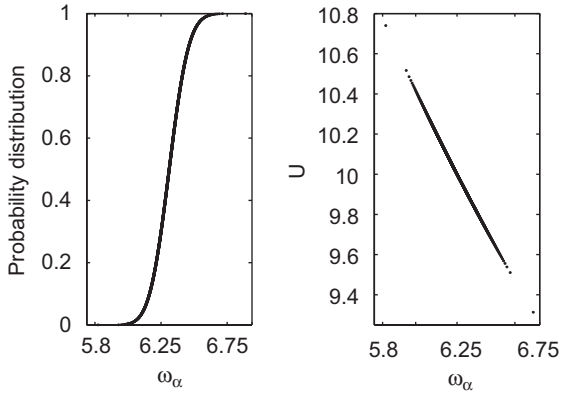

Fig. 3. Lognormal distribution of ω_α for $\mu_{\omega_\alpha} = 6.25\,\text{rad/s}$ and $CV_{\omega_\alpha} = 1.5\%$.

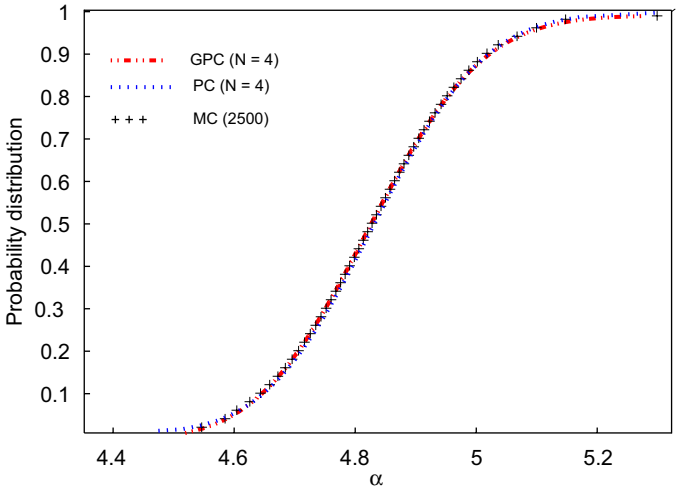

Fig. 4. Probability distribution of response α^0 for $\mu_{\omega_\alpha} = 6.25\,\text{rad/s}$ and $CV_{\omega_\alpha} = 1.5\%$.

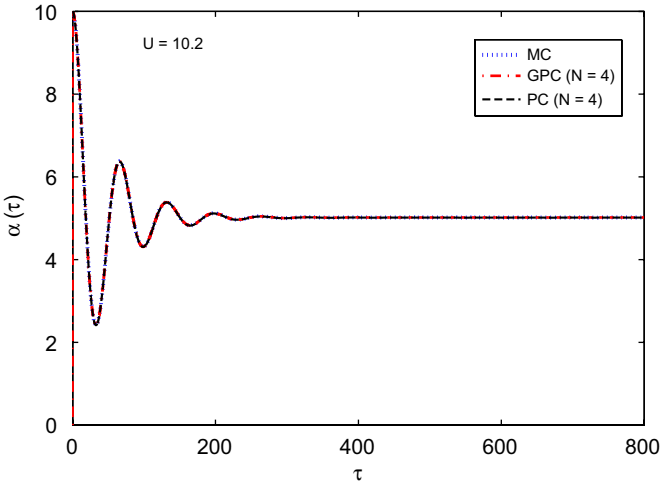

Fig. 5. Comparison of a typical time history for $\mu_{\omega_\alpha} = 6.25\,\mathrm{rad/s}$, $CV = 1.5\%$.

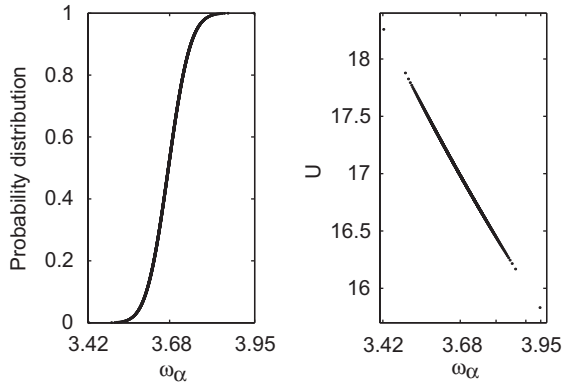

Fig. 6. Lognormal distribution of ω_α for $\mu_{\omega_\alpha} = 3.68\,\mathrm{rad/s}$ and $CV_{\omega_\alpha} = 1.5\%$.

In Fig. 5 the reconstruction of a typical time history from the GPC and PC results is compared with the deterministic realization for $U = 10.2$ in the lower tail of the probability distribution of ω_α. The response $\alpha(\tau)$ stays below the stall angle of 12° and shows a decaying solution as expected. The reconstructed time histories match accurately with the deterministic realization.

4.1.2. Uncertain pitch natural frequency ω_α in the post-bifurcation domain

For the post-bifurcation case the mean of the pitch natural frequency ω_α is given by $\omega_\alpha = 3.68\,\mathrm{rad/s}$, which corresponds to $U = 17$ using the test data of $\bar{V} = 50\,\mathrm{m/s}$ and $b = 0.8\,\mathrm{m}$. In Fig. 6 the probability distribution of ω_α and the variation of U is shown. The realizations of U are well in the deterministic post-bifurcation range, see Fig. 2. In Fig. 7 the results of GPC, PC and MC simulation are presented in terms of the minimum and maximum values of the oscillating periodic response, $\alpha_{\min}$ and $\alpha_{\max}$, during one period as function of ω_α. GPC response results are compared for increasing expansion order $N = \{2, 4, 8\}$ in Fig. 8. The GPC method with $N = 2$ results in an inaccurate representation of the response. For increasing N the results become better and for $N = 8$ the approximation matches the MC results almost exactly (Fig. 7). The PC results match both with the GPC results for $N = 8$ and the MC simulation results.

The approximation of a typical time history for $U = 17.3$, is shown in Fig. 9. It is known that polynomial chaos expansions have difficulty resolving a periodic time history, because of the increasing nonlinearity of the response for long-term time integration (Pettit and Beran, 2006). The low order polynomial chaos expansion with $N = 2$ falls indeed short in modeling the periodic response after short-term time integration at $\tau = 300$. It has been reported by Pettit and Beran (2006) and Wan and Karniadakis (2006b) that increasing the polynomial chaos order does not increase the

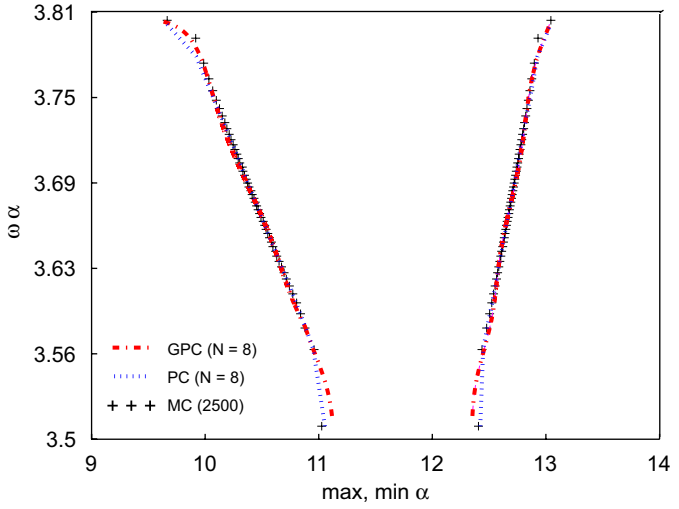

Fig. 7. Response of the maximum and minimum α^0 for $\mu_{\omega_\alpha} = 3.68\,\text{rad/s}$ and $CV_{\omega_\alpha} = 1.5\%$.

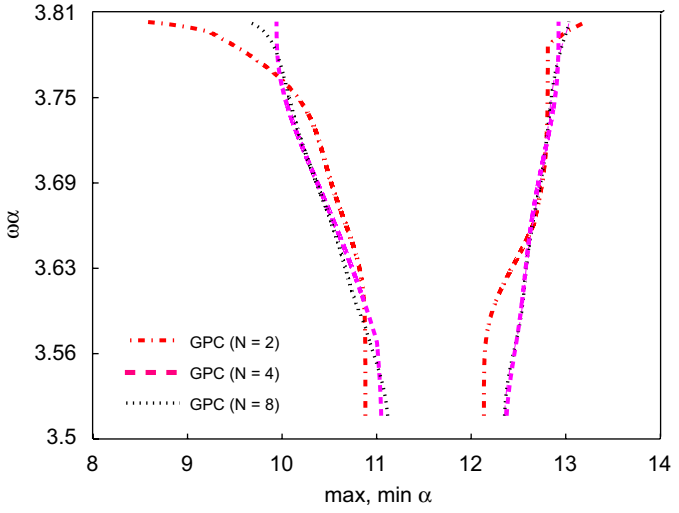

Fig. 8. Response of the maximum and minimum α^0 for $\mu_{\omega_\alpha} = 3.68\,\text{rad/s}$ and $CV_{\omega_\alpha} = 1.5\%$ with increasing order of GPC.

accuracy significantly. However, in this case a relatively small increase of the order of the expansion to $N = 8$ results in an accurate prediction of the time series up till $\tau = 800$. This could be attributed to the relatively small effect of uncertain ω_α on the frequency of the system response (Wan and Karniadakis, 2006b).

The accuracy of the GPC method and the PC method of the same order N is comparable. The relative computational efficiency of the methods is compared to that of MC simulation in Table 1. For an MC simulation of comparable accuracy up to $\tau = 500$ a number of 2500 realizations is employed. For the pre-bifurcation case of Section 4.1.1, both methods are at least a factor 40 faster than the standard MC technique, for which it takes approximately 4.5 h to complete the 2500 deterministic simulations. The computational time for solving the coupled equations in GPC is for this case relatively close to that of the nonintrusive PC, because explicit time integration is used and the system response remains in the linear pre-stall domain.

The nonlinear stall model containing nonpolynomial step function nonlinearity is important in the post-bifurcation domain. The CPU time for the PC approach is not affected significantly by the nonlinear terms. PC uses nine deterministic runs only and the post-processing using the Lagrange polynomial chaos is also not much time consuming. In contrast, GPC becomes slower by a factor of 75 compared to the pre-bifurcation case. This is caused by numerical

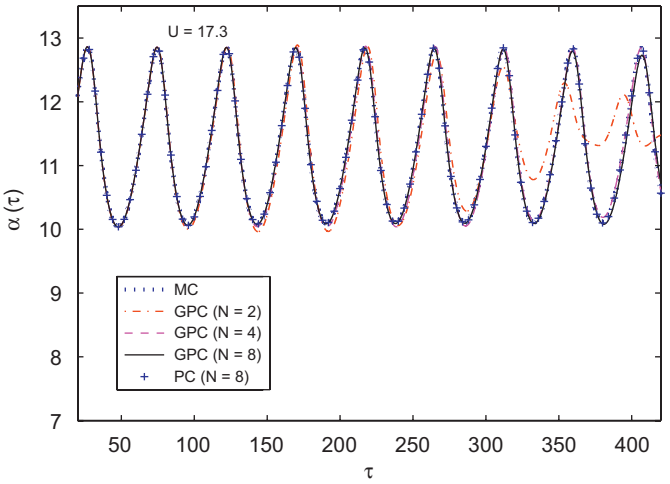

Fig. 9. Comparison of a typical time history for $\mu_{\omega_\alpha} = 3.68\,\mathrm{rad/s}$ and $CV = 1.5\%$.

Table 1
Comparison of the order of the CPU times by Galerkin polynomial chaos, probabilistic collocation and Monte Carlo simulation till $\tau = 500$

	GPC	PC	MC
Pre-bifurcation	7 min ($N = 4$)	2 min ($N = 4$)	$\approx$ 4.5 h (2500 realizations)
Post-bifurcation	8.9 h ($N = 8$)	3 min ($N = 8$)	$\approx$ 4.5 h (2500 realizations)

integration of the inner products containing the nonlinear terms at every time level. For this highly nonlinear case GPC is even twice as slow as MC simulation. These results demonstrate for this case an decrease of computational time of two orders of magnitude for PC compared to GPC. Therefore, in the rest of this paper the PC approach is used.

4.2. Uncertain cubic structural nonlinearity parameter K_{nl}

In the earlier part, the structural nonlinearity parameter K_{nl} was assumed to be zero. In this section, K_{nl} is nonzero and assumed to be uncertain described by a lognormal distribution with a mean of $\mu_{K_{\mathrm{nl}}} = 0.001$ and a CV of $CV_{K_{\mathrm{nl}}} = 15\%$. The effect on the overall bifurcation behavior of the system with respect to bifurcation parameter U is considered. Due to the high CV at least 15 collocation points are required in order to achieve convergence. This is rather high compared to the previous case where a maximum of nine points were used (corresponding to order 8). However, the coefficient of variation $CV_{K_{\mathrm{nl}}}$ is higher than the earlier case which requires such a choice in order to match deterministic solutions. A convergence study was performed in such a way that time histories corresponding to 99.8% of the domain match with that of deterministic results. This results in a minimum value of 15 collocation points; below which PC results show discrepancies with the deterministic solution.

The bifurcation diagram with the 99.8% uncertainty bars is shown in Fig. 10. The bifurcation parameter U is varied with 0.05 intervals between $U = 15.5$ and 16.5. With this resolution the closest estimate of the shift of the supercritical Hopf bifurcation point due to the nonzero nonlinear stiffness indicated in the figure is at $U_{cr} = 15.85$. Above the bifurcation point the systems exhibits LCOs and below $U = 15.85$ the response shows damped oscillations or stable fixed points. The uncertainty bar suggests that the overall effect of the uncertainty in the structural nonlinearity parameter K_{nl} on the bifurcation behavior is weak. The effect is smallest for the post-bifurcation values of $\alpha_{\max}$.

In Fig. 11 a zoom of the critical range of U with smaller intervals of 0.01 is shown. In this plot it is examined whether a shift in the stall flutter boundary occurs as a result of the uncertainty in K_{nl}. To that end the bifurcation plot for three realizations for $\omega = \{0.002; 0.5; 0.998\}$ are reconstructed from the PC results. The ω value of 0.5 corresponds to the median of uncertain parameter K_{nl} and the two other realizations correspond to two realizations in the tails. The figure indicates that the effect of the uncertainty in K_{nl} on the stall flutter boundary is small. The flutter boundary shifts from $U = 15.81$ to 15.83 between the three branches.

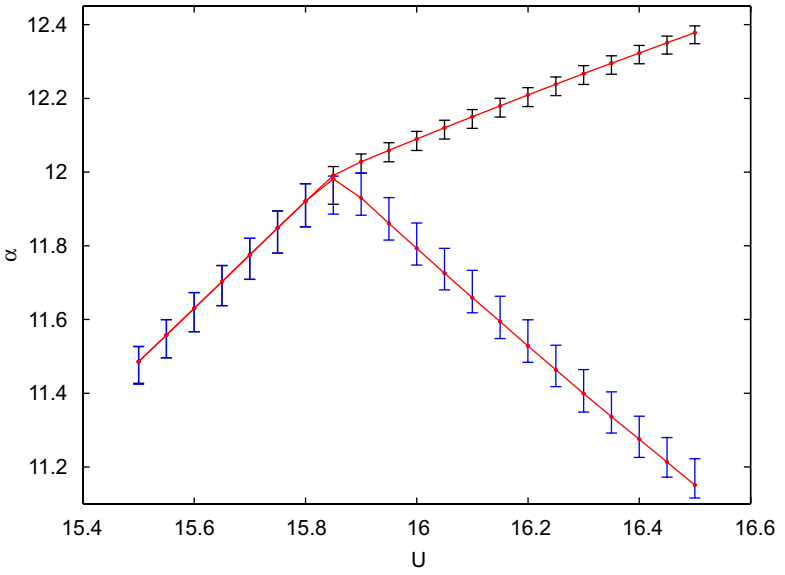

Fig. 10. Response 99.8% uncertainty bars for $\mu_{K_{\rm nl}} = 0.001$ and $CV_{K_{\rm nl}} = 15\%$.

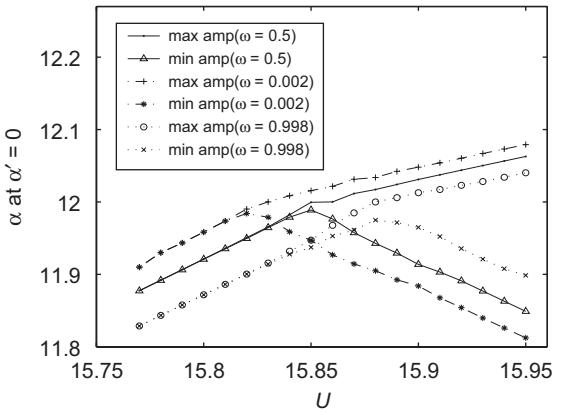

Fig. 11. Stall flutter boundaries shown as spanned in the uncertainty domain for $\mu_{K_{\rm nl}} = 0.001$ and $CV_{K_{\rm nl}} = 15\%$.

4.3. Uncertain structural equilibrium angle α_m

The structural equilibrium angle α_m (Fragiskatos, 1999) is considered to be uncertain with a mean $\mu_{\alpha_m} = 4^\circ$, a CV of $CV_{\alpha_m} = 15\%$ and a lognormal distribution. The number of collocation points is chosen as 15 following a convergence study similar to the earlier case. The bifurcation plot with 99.8% uncertainty bars is shown in Fig. 12. In the post-bifurcation domain both the minimum and maximum response, and thus the amplitude of the periodic response, are sensitive to the system parametric uncertainty. The uncertain α_m has the largest effect on the minimum response $\alpha_{\min}$ in the post-bifurcation domain, which is demonstrated by the uncertainty bars with length 6°. The resulting uncertain maximum response $\alpha_{\max}$ in the post-bifurcation domain is described by a 3° uncertainty bar. The uncertainty bar in the pre-bifurcation domain has a length of 4°.

In Figs. 13–15 the probability distribution function and probability density function of the response are presented at three characteristic U values $U = \{12.5; 15.5; 21\}$ to identify the bifurcation trend in the probability density function. At $U = 12.5$, shown in Fig. 13, the response is damped in the entire domain. For that case the probability density of the damped response shows a maximum around $\alpha = 7.3^\circ$.

For $U = 15.5$ shown in Fig. 14 both damped and oscillatory realizations are present. This results in a clearly nonlinear propagation of uncertainty to the response. Due to the oscillatory realizations

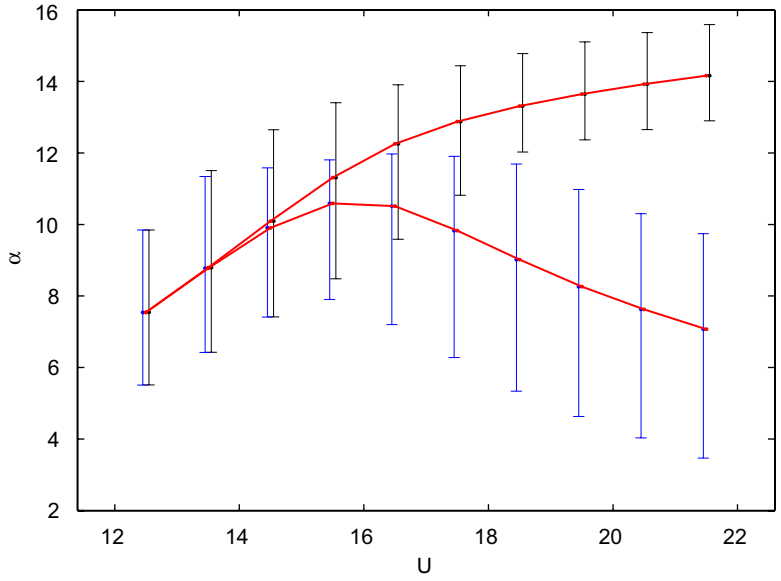

Fig. 12. Response 95% uncertainty bars for $\mu_{\alpha_m} = 4^\circ$ and $CV_{\alpha_m} = 15\%$.

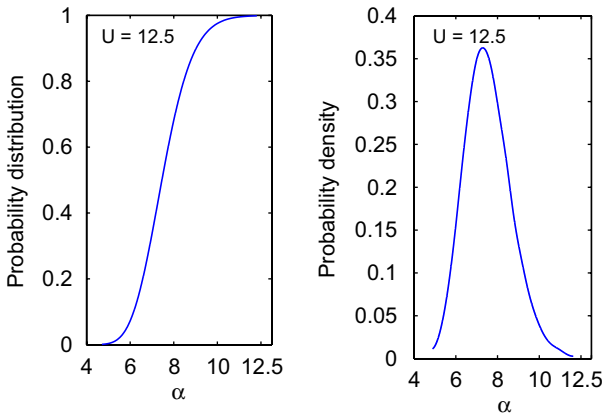

Fig. 13. Probability distribution and density of the damped response at $U = 12.5$ for $\mu_{\alpha_m} = 4^\circ$ and $CV_{\alpha_m} = 15\%$.

the system shows different values for the minimum and maximum response. The probability density of $\alpha_{\min}$ is highly deformed due to the nonmonotonic dependence on α_m. The probability of $\alpha_{\max}$ shows a maximum around 12.3°.

A third type of behavior is encountered further at $U = 21$. In that case, the entire domain shows oscillatory behavior. As a result, both the maximum and the minimum response exhibit monotonic behavior as function of α_m. The probability density functions of the minimum and maximum response show two clearly distinguishable maxima, shown in Fig. 15. The probability of the minimum response has a maximum around 7.7° and the maximum response around 13.9°. These results are summarized in Fig. 16 in the form of a bifurcation diagram in combination with three realizations for $\omega = \{0.002; 0.5; 0.998\}$. The minimum and maximum response show qualitatively different probability density functions in different bifurcation domains. Near the deterministic bifurcation point of $U = 16$ the effect of the parametric uncertainty on the response is most nonlinear.

The uncertainty in the structural equilibrium angle α_m also affects the position of the flutter point. In Fig. 17 the probability distribution of the bifurcation point is given. Based on the probability distribution it can be concluded that the flutter point is reduced by 12.5% to $U = 14$ due to the uncertain α_m, if a 5% probability of flutter is deemed

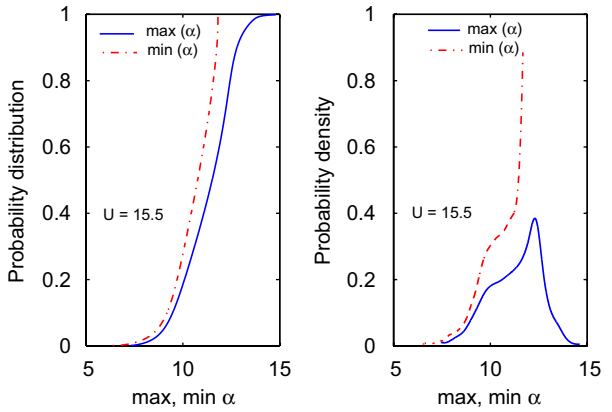

Fig. 14. Probability distribution and density of the maximum and minimum response at $U = 15.5$ for $\mu_{\alpha_m} = 4^\circ$ and $CV_{\alpha_m} = 15\%$.

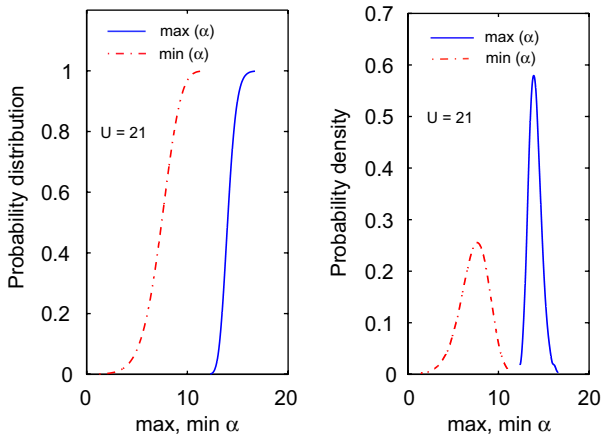

Fig. 15. Probability distribution and density of the LCO response at $U = 21$ for $\mu_{\alpha_m} = 4^\circ$ and $CV_{\alpha_m} = 15\%$.

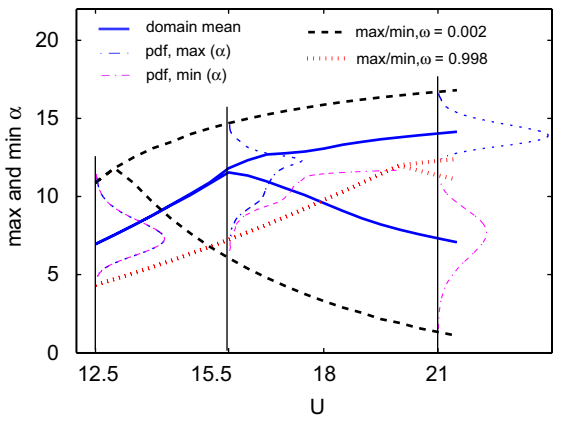

Fig. 16. Qualitative changes shown in the response probability density at three characteristic U values for $\mu_{\alpha_m} = 4^\circ$ and $CV_{\alpha_m} = 15\%$.

acceptable. This demonstrates the importance of the probabilistic modeling of uncertainties in the analysis of pitching stall flutter, since this approach can quantify the earlier onset of unstable behavior compared to the deterministic bifurcation point in a probabilistic sense.

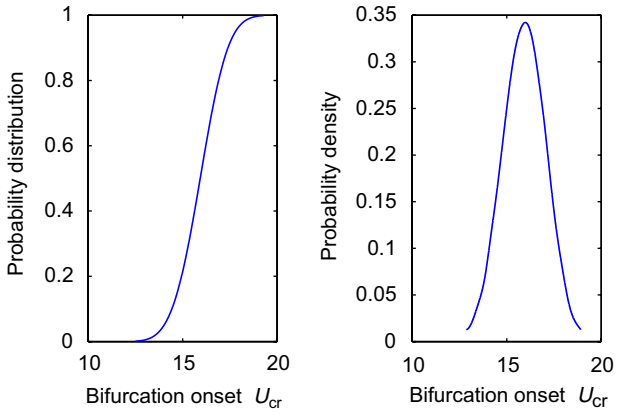

Fig. 17. Probability distribution and density of the bifurcation point for $\mu_{\alpha_m} = 4^\circ$ and $CV_{\alpha_m} = 15\%$.

5. Concluding remarks

The bifurcation behavior of pitching airfoil stall flutter subject to uncertain variation of system parameters is studied. The structure is modeled as a two-dimensional rigid airfoil with cubic nonlinear torsional stiffness. The ONERA dynamic stall model is used to compute the aerodynamic loading. An uncertain pitch natural frequency ω_α, cubic structural nonlinearity parameter K_{nl}, and structural equilibrium angle α_m are considered.

The problem is a simple model problem to understand the mechanism of stall flutter in a stochastic framework. The choice of the uncertain parameters is, however, more practical. The parameters which have been assumed to be random are torsional frequency ω_α which is determined from laboratory dynamical experiments and it could encounter various sources of uncertainty based on the laboratory conditions. K_{nl} stands for various sources of analytic nonlinearities. According to some aeroelasticity literature (Lee and Tron, 1989; Tang and Dowell, 1993b), these often represents different control mechanisms. Therefore K_{nl} could face modeling uncertainties. Similarly there could be uncertain sources of error in implementing the structural equilibrium angle.

The Galerkin polynomial chaos method and the probabilistic collocation method are applied to propagate the uncertainty through the system. The focus of this work is to investigate the success of these techniques for a stall flutter problem in linear and nonlinear regime and also with high level of uncertainty. It was to see how the flutter stability characteristics are altered due to these effects. The choice of some of the parameters like the coefficient of variation (CV) is made so as to make the system adequately sensitive to the uncertain variation of the chosen parameters.

The results of both methods are compared to an MC reference solution for the case with uncertainty in the pitch natural frequency ω_α. In the pre-bifurcation domain the polynomial chaos methods are both significantly more efficient than MC simulation. The computational costs of the GPC method in the post-bifurcation domain are of the same order as MC simulation owing to the nonpolynomial nonlinearity of the model above the static stall angle. The bifurcation does not affect the computational costs of the PC method significantly. In the post-bifurcation case low order polynomial chaos expansions fail to predict the periodic response after short-term time integration up to $\tau = 300$. An eighth order polynomial chaos expansion is sufficient to maintain an accurate solution till around $\tau = 800$, well after the system reaches time stationarity.

The effect of the uncertain cubic structural nonlinearity parameter K_{nl} and structural equilibrium angle α_m are studied using the PC method. Uncertainty in α_m has the largest effect on the bifurcation behavior of the system. It results in 3–6° uncertainty bars for the response, which affects the amplitude of the periodic response in the post-bifurcation domain. The minimum and maximum response show qualitatively different probability density functions at different domains of the bifurcation plot. The uncertainty in α_m results in a flutter point which is 12.5% lower than the deterministic prediction if 5% probability of flutter is deemed acceptable. This demonstrates that parametric uncertainties in pitching airfoil stall flutter can lead to an earlier onset of unstable behavior than a deterministic analysis would point out.

This study successfully uses the uncoupled and nonintrusive PC approach to quantify the effect of uncertain parametric variation of a stall flutter system. The stall flutter model is simple and yet can predict the nature of instabilities that can occur in an actual system. Therefore, the stochastic modeling of the present system will be helpful

towards the aeroelastic design of a real-life stall flutter device without being too computationally intensive. In this work, the PC approach is used to capture the period-1 LCOs. As a next step, we would like to investigate capturing higher periodic responses as well.

References

Babuska, I.M., Nobile, F., Tempone, R., 2007. A stochastic collocation method for elliptic partial differential equations with random input data. SIAM Journal on Numerical Analysis 45 (3), 1005–1034.

Beedy, J.A., Barakos, G., Badcock, K.J., Richards, B.E., 2003. Nonlinear analysis of stall flutter based on the ONERA aerodynamic model. The Aeronautical Journal 107 (1074), 495–509.

Beloiu, D.M., Ibrahim, R.A., Pettit, C.L., 2005. Influence of boundary conditions relaxation on panel flutter with compressive in-plane loads. Journal of Fluids and Structures 21, 743–767.

Bhattacharya, R., Waymire, E.C., 2007. A Basic Course on Probability Theory. Springer, Berlin.

Cheney, M.C., Migliore, P.G., 2000. Feasibility study of pultruded blades for wind turbine rotors. In: 38th Aerospace Sciences Meeting and Exhibit, Reno, NV, USA, Paper no. AIAA-2000-0061.

Choi, S., Namachchivaya, N.S., 2006. Stochastic dynamics of a nonlinear aeroelastic system. AIAA Journal 44 (9), 1921–1931.

De Rosa, S., Franco, F., 2008. Exact and numerical responses of a plate under a turbulent boundary layer excitation. Journal of Fluids and Structures 24, 212–230.

Debusschere, B.J., Najm, H.N., Pébay, P., Knio, O.M., Ghanem, R.G., LeMaître, O.P., 2004. Numerical challenges in the use of polynomial chaos representations for stochastic processes. SIAM Journal on Scientific Computing 26, 698–719.

Dowell, E.H., Curtiss, H.C.J., Scanlan, R.H., Sisto, F., 1989. A Modern Course in Aeroelasticity. Kluwer Academic Publisher, Dordrecht.

Dunn, P., Dugundji, J., 1992. Nonlinear stall flutter and divergence analysis of cantilevered graphite/epoxy wings. AIAA Journal 30 (1), 153–162.

Fragiskatos, G., 1999. Nonlinear response and instabilities of a two-degree-of-freedom airfoil oscillating in dynamic stall. M.Eng. Masters Thesis, McGill University, Montreal, Canada.

Fung, Y.C., 1955. An Introduction to the Theory of Aeroelasticity. Wiley, New York.

Ganappathysubramanian, B., Zabaras, N., 2007. Sparse grid collocation schemes for stochastic natural convection problems. Journal of Computational Physics 225, 652–685.

Gautschi, W., 2004. Orthogonal Polynomials; Computation and Approximation. Oxford University Press, Oxford.

Gautschi, W., 2005. Orthogonal polynomials (in matlab). Journal of Computational and Applied Mathematics 178, 215–234.

Gerstner, T., Griebel, M., 1998. Numerical integration using sparse grids. Numerical Algorithms 18, 209–232.

Ghanem, R., 1999. Stochastic finite elements with multiple random non-Gaussian properties. Journal of Engineering Mechanics 125, 26–40.

Ghanem, R.G., Spanos, P., 1991. Stochastic Finite Elements: A Spectral Approach. Springer, New York.

Golub, G.H., Welsch, J.H., 1969. Calculation of gauss quadrature rules. Mathematics of Computation 23, 221–230.

Hosder, S., Walters, R.W., Perez, R., 2006. A non-intrusive polynomial chaos method for uncertainty propagation in CFD simulations. In: 44th AIAA Aerospace Sciences Meeting and Exhibit, Reno, NV, USA, Paper no. AIAA-2006-891.

Ibrahim, R.A., Beloiu, D.M., Pettit, C.L., 2005. Influence of joint relaxation on deterministic and stochastic panel flutter. AIAA Journal 43 (7), 1444–1454.

Le Maître, O.P., Knio, O.M., Najm, H.N., Ghanem, R.G., 2004. Uncertainty propagation using Wiener–Haar expansions. Journal of Computational Physics 197, 28–57.

Lee, B.H.K., Tron, A., 1989. Effects of structural nonlinearities on flutter characteristics of the cf-18 aircraft. Journal of Aircraft 26 (8), 781–786.

Lee, B.H.K., Price, S.J., Wong, Y.S., 1999. Nonlinear aeroelastic analysis of airfoils: bifurcation and chaos. Progress in Aerospace Sciences 35, 205–334.

Liaw, D.G., Yang, H.T.Y., 1993. Reliability and nonlinear supersonic flutter of uncertain laminated plates. AIAA Journal 31 (12), 2304–2311.

Lind, R., Brenner, M.J., 1998. Robust flutter margin analysis that incorporates flight data. NASA/TP-1998-206543.

Lindsley, N.J., Beran, P.S., Pettit, C.L., 2002. Effects of uncertainty on nonlinear plate aeroelastic response. In: 43rd AIAA/ASME/ASCE/AHS/ASC Structures, Structural Dynamics, and Materials Conference, Denver, CO, USA, Paper no. AIAA 2002-1271.

Lindsley, N.J., Pettit, C.L., Beran, P.S., 2006. Nonlinear plate aeroelastic response with uncertain stiffness and boundary conditions. Structure and Infrastructure Engineering 2, 201–220.

Loeven, G., Witteveen, J.A.S., Bijl, H., 2007. Probabilistic collocation: an efficient non-intrusive approach for arbitrarily distributed parametric uncertainties. In: 45th AIAA Aerospace Sciences Meeting and Exhibit, Reno, NV, USA, Paper no. AIAA-2007-317.

Lucor, D., Karniadakis, G.E., 2004. Noisy inflows cause a shedding-mode switching in flow past an oscillating cylinder. Physical Review Letters 92, 4501.

Mathelin, L., Hussaini, M.Y., 2003. A stochastic collocation algorithm for uncertainty analysis. Technical Report NASA/CR-2003-212153, NASA Langley Research Center.

Mathelin, L., Hussaini, M.Y., Zang, T.A., 2005. Stochastic approaches to uncertainty quantification in CFD simulations. Numerical Algorithms 38, 209–236.

Millman, D.R., King, P.I., Beran, P.S., 2003. A stochastic approach for predicting bifurcation of a pitch and plung airfoil. In: 21st AIAA Applied Aerodynamics Conference, Orlando, FL, USA, Paper no. AIAA-2003-3515.

Nigam, N.C., Narayanan, S., 1994. Applications of Random Vibrations. Narosa Publishing House, New Delhi.

Pettit, C.L., 2004a. Uncertainty in aeroelasticity analysis, design and testing. In: Nicolaidis, E., Ghiocel, D. (Eds.), Engineering Design Reliability Handbook. CRC Press, Boca Raton, FL.

Pettit, C.L., 2004b. Uncertainty quantification in aeroelasticity: recent results and research challenges. Journal of Aircraft 41 (5), 1217–1229.

Pettit, C.L., Beran, P.S., 2004. Polynomial chaos expansion applied to airfoil limit cycle oscillations. In: 45th AIAA/ASME/ASCE/AHS/ASC Structures, Structural Dynamics and Materials Conference, California, Paper no. AIAA 2004-1691.

Pettit, C.L., Beran, P.S., 2006. Spectral and multiresolution wiener expansions of oscillatory stochastic process. Journal of Sound and Vibration 294, 752–779.

Poirel, D., Price, S.J., 2003. Random binary (coalescence) flutter of a two-dimensional linear airfoil. Journal of Fluids and Structures 18, 23–42.

Poirion, F., 2000. On some stochastic method applied to aeroservoelasticity. Aerospace Science and Technology 4, 201–214.

Price, S.J., Fragiskatos, G., 2000. Nonlinear aeroelastic response of a two-degree-of-freedom airfoil oscillating in dynamic stall. In: Ziada, S., Staubli, T. (Eds.), Proceedings of Flow Induced Vibration. Balkema, Rotterdam.

Reagan, M.T., Najm, H.N., Ghanem, R.G., Knio, O.M., 2003. Uncertainty quantification in reacting-flow simulations through non-intrusive spectral projection. Combustion and Flame 132, 545–555.

Sarkar, S., Bijl, H., 2008. Nonlinear aeroelastic behavior of an oscillating airfoil during stall induced vibration. Journal of Fluids and Structures 24 (6), 757–777.

Sheta, E.F., Harrand, V.J., Thompson, D.E., W., S.T., 2002. Computational and experimental investigation of limit cycle oscillations of nonlinear aeroelastic systems. Journal of Aircraft 39(1), 133–141.

Stiesdal, H., 1999. The wind turbine components and operation. Bonus-Info, Newsletter ⟨http://www.windmission.dk/workshop/BonusTurbine.pdf⟩.

Svácek, P., Feistauer, M., Horácek, J., 2007. Numerical simulation of flow induced airfoil vibrations with large amplitudes. Journal of Fluids and Structures 23, 391–411.

Tang, D.M., Dowell, E.H., 1993a. Comparison of theory and experiment for nonlinear flutter and stall response of a helicopter blade. Journal of Sound and Vibration 165 (2), 251–276.

Tang, D.M., Dowell, E.H., 1993b. Nonlinear aeroelasticity in rotorcraft. Mathematical and Computer modelling 18, 157–184.

Tang, D.M., Dowell, E.H., 2004. Effects of geometric structural nonlinearity on flutter and limit cycle oscillations of high-aspect-ratio wings. Journal of Fluids and Structures 19, 291–306.

Tran, C.T., Petot, T., 1981. Semi-empirical model for the dynamic stall of airfoils in view of the application to the calculation of responses of a helicopter blade in forward flight. Vertica 5, 35–53.

Walters, R.W., 2003. Towards stochastic fluid mechanics via polynomial chaos. In: 41st AIAA Aerospace Sciences Meeting and Exhibit, Reno, NV, USA, Paper no. AIAA-2003-0413.

Wan, X., Karniadakis, G., 2006a. Beyond Wiener–Askey expansions: handling arbitrary PDFs. Journal of Scientific Computing 27, 455–464.

Wan, X., Karniadakis, G.E., 2006b. Long-term behavior of polynomial chaos in stochastic flow simulations. Computer Methods in Applied Mechanics and Engineering 195, 5582–5596.

Wiener, N., 1938. The homogeneous chaos. American Journal of Mathematics 60, 897–936.

Witteveen, J.A.S., Bijl, H., 2006a. Modeling arbitrary uncertainties using Gram–Schmidt polynomial chaos. In: 44th AIAA Aerospace Sciences Meeting and Exhibit, Reno, NV, USA, Paper no. AIAA-2006-896.

Witteveen, J.A.S., Bijl, H., 2006b. Using polynomial chaos for uncertainty quantification in problems with nonlinearities. In: 47th AIAA/ASME/ASCE/AHS/ASC Structures, Structural Dynamics, and Materials Conference, Newport, RI, USA, Paper no. AIAA-2006-2066.

Xiu, D., Karniadakis, G.E., 2002. The Wiener–Askey polynomial chaos for stochastic differential equations. SIAM Journal on Scientific Computing 24 (2), 619–644.

Xiu, D.B., Hesthaven, J.S., 2005. High-order collocation methods for differential equations with random inputs. SIAM Journal on Scientific Computing 27, 1118–1139.